

Activity variation driven by flux emergence and transport on Sun-like stars

Emre Işık,^{1,2} Sami K. Solanki,^{1,3} Natalie A. Krivova,¹ Alexander I. Shapiro,¹

¹ Max-Planck-Institut für Sonnensystemforschung, Justus-von-Liebig-Weg 3, 37077, Göttingen, Germany

² Feza Gürsey Center for Physics and Mathematics, Boğaziçi University, 34680 Kuleli, Istanbul, Turkey

³ School of Space Research, Kyung Hee University, Yongin, Gyeonggi-Do, 446-701, Republic of Korea

Abstract

In G dwarfs, the surface distribution, coverage and lifetimes of starspots deviate from solar-like patterns as the rotation rate increases. We set up a numerical platform which includes the large-scale rotational and surface flow effects, aiming to simulate evolving surface patterns over an activity cycle for up to 8 times the solar rotation and flux emergence rates. At the base of the convection zone, we assume a solar projected butterfly diagram. We then follow the rotationally distorted trajectories of rising thin flux tubes to obtain latitudes and tilt angles. Using them as source distributions, we run a surface flux transport model with solar parameters. Our model predicts surface distributions of the signed radial fields and the starspots that qualitatively agree with observations.

1 Introduction

Sun-like stars exhibit magnetically induced brightness and spectropolarimetric variability in a broad range of timescales. Rotational variations are induced by starspots whereas annual to decadal variations are potentially driven by activity cycles and/or by long-term effects of short-term stochasticity. Physical models of the surface distribution of magnetic activity on Sun-like stars can help us gain insight to better characterise physical processes involved. They can also be used in forward-modelling of brightness variations and compare with space-borne photometry.

We developed a modelling platform to simulate large-scale magnetic fields over the stellar surface and in time (Işık *et al.*, 2018). Here we present a summary of the method and a selection of simulation results for a set of rotation rates and activity levels.

2 Emergence of magnetic flux

We take a Sun-like butterfly diagram of flux eruptions to represent initial latitudes of thin flux tubes and follow their buoyant rise up to the surface, to obtain the emergence latitudes and tilt angles at the surface. We follow the procedure outlined below, to set up the pattern of magnetic flux eruptions from the base of the convection zone.

1. Magnetic flux eruptions from the base of the convection zone follow a statistical numerical model of the activity cycle at the solar surface (Jiang *et al.*, 2011a). To simulate the rotation-activity relation, we set the flux emergence frequency (in solar units) equal to the stellar rotation rate (in solar units).
2. Emergence latitude and tilt angle for a given eruption are calculated from numerical simulations of thin flux tubes rising through a non-local mixing-length solar convection zone stratification.

3. The initial field strength of a flux tube is set by a function of the initial latitude. This function is determined by the linear stability condition for mechanical equilibrium of a thin flux ring in the convective overshoot region, for given stellar rotation rate. We take a linear growth time of 50 days for any flux tube. In this way, the field strength is close to the critical strength for the onset of magnetic buoyancy instability. We assume that the latitudinal and radial differential rotation amplitudes ($\Delta\Omega$) do not change for faster rotation.
4. The nonlinear flux-tube simulations are stopped when the thin-flux-tube condition is violated, i.e., at about $0.98R_{\odot}$. The emergence latitude is recorded at this point. The tilt angle is calculated from the coordinates of the legs of the flux loop at $0.97R_{\odot}$.

3 Transport of surface magnetic flux

We take the emergence latitudes and tilt angles resulting from the procedure described above into a surface flux transport (SFT) model (see also Işık *et al.*, 2011). On top of the emergence model, we modify the emergence latitudes and longitudes in a probabilistic way, so as to allow for nesting of activity. In the current work, we defined only a single activity cycle and we did not impose random scatter about the tilt angles, which we derived from rising flux tubes.

For the SFT parameters, we adopt values which were calibrated for simulations of solar activity for observed solar cycles (Jiang *et al.*, 2011b). The resulting longitudinally averaged signed and unsigned magnetic fields are shown in Fig. 1, for the solar case and eight times more rapid rotation (also eight times more frequent emergence). For the latter case, the polar fields attain strengths comparable with the lower-latitude fields. The activity belts are also shifted towards higher latitudes, owing to increasing poleward deflection of rising flux tubes by the Coriolis effect. Formation of

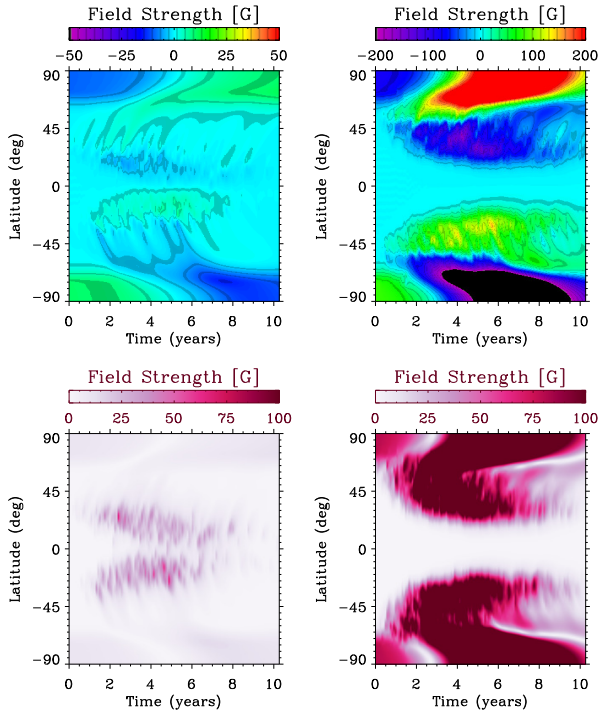


Figure 1: Azimuthal averages of signed (upper panels) and unsigned (lower panels) field strength, as a function of time, for solar (left) and eight times solar (right) rotation rate.

strong polar caps are also affected by increasing tilt angles of emerging bipolar regions, hence increasing dipole-moment contributions to the global (axial) dipole.

4 Modelling spot coverages

As a first approximation to estimate starspot distributions, we set a threshold field strength, above which every pixel in the simulated magnetic map is treated as belonging to starspots. We determined the threshold value by requiring that the cycle-averaged global sunspot area coverage is about 0.2%, representing a moderate to strong activity cycle. We then applied this criterion to our set of models with rotation rates 1 to 8 times that of the Sun.

Figure 2 shows the evolution of the global spot coverage in the course of the activity cycle for given rotation rate (note that the activity level was assumed to scale linearly with the rotation rate). Our models correspond to sidereal rotation periods of about 25, 12, 6, and 3 days, for which we assumed 1, 2, 4, and 8 times more frequent emergence than on the Sun. The area distribution of bipolar regions was kept unchanged. Among the models, the ‘8x’ case deviates substantially from others, reaching spot coverages comparable to the lowest disc coverages observed for the G1.5V-type star EK Draconis, which rotates 9 times faster than the Sun (O’Neal *et al.*, 2004).

5 Effect of nests of activity

It is known that sunspot groups tend to emerge near sites of recent flux emergence. Statistics of such active nests were thoroughly investigated for the Sun (e.g., Castenmiller *et al.*,

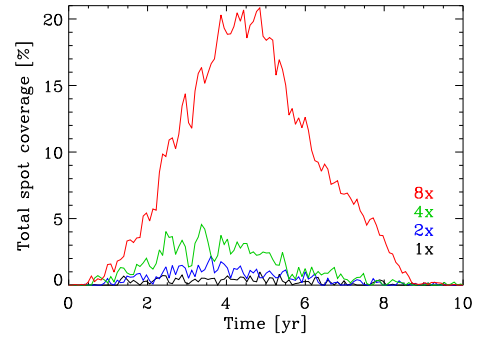


Figure 2: Cycle variation of the area covered by spots, for 1 to 8 times the solar rotation rate.

1986; Pelt *et al.*, 2010). Our knowledge of the degree of nesting on other stars is currently limited by the low spatial resolution encountered in observational reconstructions of stellar surfaces. In the next stages of this project, we plan to reconstruct disc-integrated brightness variations out of our simulations. Such forward modelling can be useful in estimating the degree of starspot nesting from observations.

We included a nesting feature in the model by setting a probability for a given emergence to occur nearby recent emergence events. We assumed the probability that a given emerging bipolar region becomes a nest centre or that it belongs to a pre-existing nest to be 70%. Figure 3 shows pole-on views from the ‘8x’ simulations, with and without nesting. By visual inspection we can already assess that nesting can have a large impact on the longitudinal distribution of spots on active stars. The amplitude of rotational brightness variations would be significantly larger in the nested case as compared to a spot distribution with random longitudes. In addition, photometric detection of starspots would also be easier when they are nested, because smaller spots that are individually below a given detection threshold can be more easily detected when they are clustered, i.e., when they are more or less in phase and form a stronger photometric signal.

6 Summary and outlook

We developed a model that calculates the surface distribution of radial magnetic field and starspots on Sun-like stars for a range of rotation periods between that of the Sun down to 3 days. The model assumes a one-to-one relation between the rotation rate and the flux emergence frequency, which is roughly consistent with empirical relations. This is in fact a free parameter that can be adjusted according to a desired observational relation.

Our results suggest that polar spots should start to form close to about $P_{\text{rot}}=3$ days. In our models, this happens due to the enhanced flux emergence rate and increased tilt angles. Consequently, the ‘polar spot’ is largely unipolar, but it is surrounded by the opposite-polarity flux at high latitudes, where starspots can form.

We plan to extend our models to multiple cycles with varying degrees of overlap, tilt angle scatter, and various possible perturbations of large-scale flows. To better describe the various variability patterns observed by the *Kepler* mission, we will also include (i) a more physical algorithm to decom-

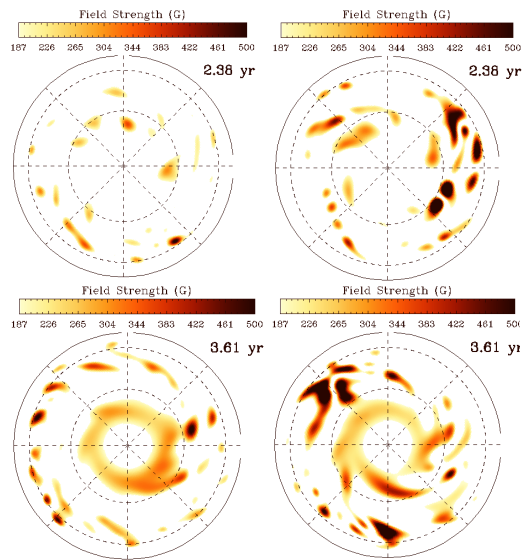


Figure 3: Pole-on snapshots of starspot distributions for a Sun-like star rotating 8 times faster than the Sun. Left: no nesting, Right: with a nesting probability of 70%.

pose the emerging magnetic field into starspots and faculae, as well as (ii) activity nesting as a function of the stellar activity level.

Acknowledgments

EI acknowledges support by the Young Scientist Award Programme BAGEP-2016 of the Science Academy, Turkey. This work has been partially supported by the BK21 plus program through the National Research Foundation (NRF) funded by the Ministry of Education of Korea. AS acknowledges funding from the European Research Council under the European Union Horizon 2020 research and innovation programme (grant agreement No. 715947).

References

- Castenmiller, M. J. M., Zwaan, C., & van der Zalm, E. B. J. 1986, *SoPh*, 105, 237.
- Işık, E., Schmitt, D., & Schüssler, M. 2011, *A&A*, 528, A135.
- Işık, E., Solanki, S. K., Krivova, N. A., & Shapiro, A. I. 2018, *A&A*, 620, A177.
- Jiang, J., Cameron, R. H., Schmitt, D., & Schüssler, M. 2011a, *A&A*, 528, A82.
- Jiang, J., Cameron, R. H., Schmitt, D., & Schüssler, M. 2011b, *A&A*, 528, A83.
- O’Neal, D., Neff, J. E., Saar, S. H., & Cuntz, M. 2004, *AJ*, 128, 1802.
- Pelt, J., Korpi, M. J., & Tuominen, I. 2010, *A&A*, 513, A48.